





SOURAV RAY¹, VIKRAM SUNKARA², CHRISTOF SCHÜTTE³ MARCUS WEBER⁴ ⁵

How to calculate pH-dependent binding rates for receptor-ligand systems based on thermodynamic simulations with different binding motifs

¹  0000-0001-5097-9825

²  0000-0002-4940-8344

³  0000-0001-5232-2683

⁴  0000-0003-3939-410X

⁵ corresponding author

Zuse Institute Berlin
Takustr. 7
14195 Berlin
Germany

Telephone: +49 30-84185-0
Telefax: +49 30-84185-125

E-mail: bibliothek@zib.de
URL: <http://www.zib.de>

ZIB-Report (Print) ISSN 1438-0064
ZIB-Report (Internet) ISSN 2192-7782

How to calculate pH-dependent binding rates for receptor-ligand systems based on thermodynamic simulations with different binding motifs

Sourav Ray³, Vikram Sunkara^{1,2}, Christof Schütte^{1,2,3}, and Marcus Weber^{3,4}

¹Dept. of Mathematics and Computer Science, Freie Universität Berlin, 14195 Berlin, Germany.

²Computational Physiology and Anatomy, Zuse Institute Berlin, 14195 Berlin, Germany.

³Computational Drug Design, Zuse Institute Berlin, 14195 Berlin, Germany.

⁴corresponding author. Email: weber@zib.de

June 2020

Abstract

Molecular simulations of ligand-receptor interactions are a computational challenge, especially when their association- (“on”-rate) and dissociation- (“off”-rate) mechanisms are working on vastly differing timescales. In addition, the timescale of the simulations themselves is, in practice, orders of magnitudes smaller than that of the mechanisms; which further adds to the complexity of observing these mechanisms, and of drawing meaningful and significant biological insights from the simulation.

One way of tackling this multiscale problem is to compute the free-energy landscapes, where molecular dynamics (MD) trajectories are used to only produce certain statistical ensembles. The approach allows for deriving the transition rates between energy states as a function of the height of the activation-energy barriers. In this article, we derive the association rates of the opioids fentanyl and N-(3-fluoro-1-phenethylpiperidin-4-yl)- N-phenyl propionamide (NFEPP) in a μ -opioid receptor by combining the free-energy landscape approach with the square-root-approximation method (SQRA), which is a particularly robust version of Markov modelling. The novelty of this work is that we derive the association rates as a function of the pH level using only an ensemble of MD simulations. We also verify our MD-derived insights by reproducing the *in vitro* study performed by the Stein Lab, who investigated the influence of pH on the inhibitory constant of fentanyl and NFEPP (Spahn et al. 2017).

MD simulations are far more accessible and cost-effective than *in vitro* and *in vivo* studies. Especially in the context of the current opioid crisis, MD simulations can aid in unravelling molecular functionality and assist in clinical decision-making; the approaches presented in this paper are a pertinent step forward in this direction.

Keywords. Opioid, Ligand-Receptor Interaction, Binding Kinetics, Molecular Dynamics, Metadynamics, SQRA.

1 Introduction into the Molecular Background

Binding rates of small molecules (ligands) to their target protein (receptor) can be strongly influenced by the pH value of the chemical environment. This observation depends on the

acidity (pKa) of the ligand, and also on whether the receptor structure changes with pH [34]. In the molecular simulation of ligand-receptor binding processes, this pHdependence must be taken into account. It can be assumed that the pH value in an ensemble of ligand-receptor molecular systems influences the probabilities for the occurrence of protonated or deprotonated titratable moieties. This leads to the question of how these probabilities should be considered within molecular simulation. One could imagine including the transport of protons in the simulation and thus also the process of protonation of individual titratable moieties. This procedure has several disadvantages. Since it can only be carried out for a certain pH value, i.e. for a certain proton concentration, and since purely molecular dynamics (MD) simulations do not depict protonation processes, quantum-theoretical aspects would have to be taken into account, which makes it very hard and often impossible to simulate large systems [17]. In addition, the binding modes of ligand-receptor complexes are often also pH-dependent, so that the simulations involving the protonation of molecular moieties would also have to take place on long time scales that allow for a statistical analysis of the different binding motifs. This in turn would mean that the simulations would have to take place over very many time scales, which in turn require a lot of computing time and often even is infeasible.

Our approach differs from this approach and is based on a the so-called square root approximation (SQRA) [31], a mathematical method for numerically solving the Fokker-Planck equation [8]. SQRA can be used efficiently in high dimensions as required in molecular simulation, and can be seen as a particularly robust version of Markov modelling [6], its variational variants [45], or similar methods well studied in molecular dynamics [26, 37].

Our idea is to simulate the different possible scenarios separately. This means taking into account the combination of protonated and deprotonated molecular moieties in the different situations. Based on this approach, it is possible to appropriately average over many individual molecular dynamics simulations, depending on how the external pH affects the probabilities for the simulated scenarios. Please note, that it is *not* correct to use weighted averages of the individual binding rates. What can be averaged, however, are the occupation probabilities of the individual intermediate steps of the binding process. SQRA offers a robust way to calculate the binding rates of the overall process from the averaged occupation numbers of the intermediate steps [31].

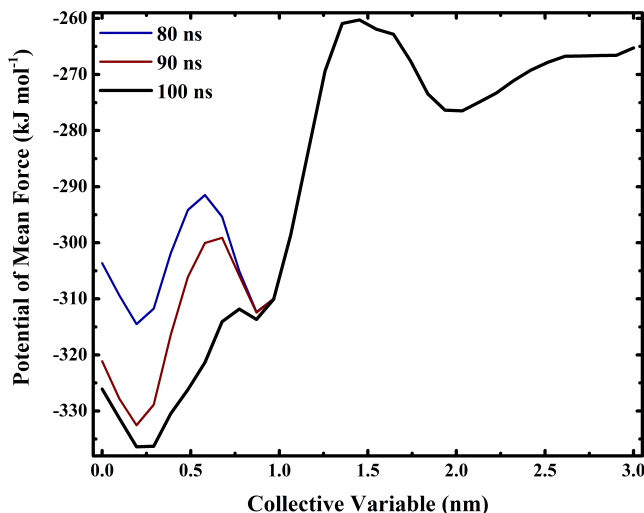


Figure 1: Potential of mean force (PMF) computed by applying a Metadynamics simulation to the following receptor-ligand system: “Fentanyl binds to the μ -opioid receptor at pH 7” (see Sec.2). The reaction coordinate represents the distance of the fentanyl molecule from its known binding site.

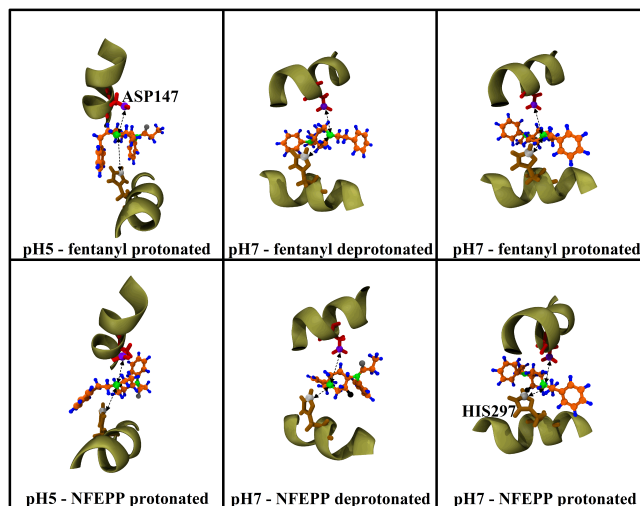


Figure 2: Binding modes

In this way, SQRA solves one challenge of the calculation of binding rates of complex systems. However, often there is another problem that makes MD simulations very troublesome or even infeasible. This additional challenge concerns the intermediate steps of the binding process, which may differ from the intermediate steps of the dissociation process.

The molecular system we will look at in this article is an analgesic molecule (fentanyl or N-(3-fluoro-1-phenethylpiperidin-4-yl)-N-phenyl propionamide (NFEPP) [40]) and the receptor it activates (μ -opioid receptor). Figure 1 shows the result of a metadynamics simulation in which the fentanyl molecule started 30 Å (3 nm) away from its binding site and has been placed at the “entrance” of the receptor. Metadynamics calculates the PMF curve of the simulated process. When the molecule is placed at the entrance of the receptor, it is pulled very quickly into the interior of the receptor, as it can then lose a large amount of free energy. Thus, the binding rate depends mainly on the last “locking” of the molecule into its final binding position. However, this part of the PMF cannot be investigated with sufficient accuracy using metadynamics simulations (different curves in Fig. 1). Therefore, in the next section we will perform separate simulations for this last binding step only. The situation is different with the dissociation of the fentanyl molecule out of the receptor.

Here the molecular system has to overcome a high PMF energy barrier (up to about 15 Å away from the binding site). We will therefore have to determine the dissociation rate in a different way. Once the binding rate is given and the binding affinity is known, the dissociation rate can be calculated from the law of mass action.

2 Methods

The structure of the μ -opioid receptor was obtained from the RCSB database (PDB: 6DDF [27]). Protonation states of the individual amino acid residues in the receptor were assigned based on calculations at pH 5 and pH 7. The protonated and deprotonated forms of fentanyl and NFEPP were sketched and parameterised using the CHARMM-GUI *Ligand Reader & Modeler* [22].

2.1 Molecular Simulations of Binding Modes

The protonated fentanyl was positioned into the μ -opioid receptor at pH 5 with the Autodock program [35]. The docking calculations were based on the Gasteiger-Marsili charges [12]. Au-

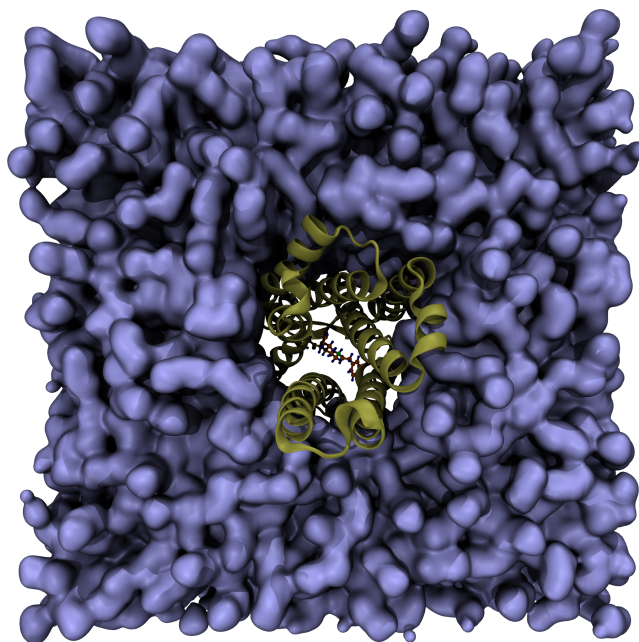


Figure 3: Our simulations take into account the μ -opioid receptor (secondary structure elements) in a membrane (blue surface), the ligand (bonds and atoms), and explicit water molecules (not shown in this figure).

togrid was used for grid preparation, with a grid spacing of 0.65 \AA , that covered the entire receptor. Ten docking runs were performed using Lamarckian genetic algorithm [36], with the rates of gene mutation and crossover kept at 0.02 and 0.8, respectively for the LUDI scoring function employed [3]. All other docking parameters were kept at their default values. The ligand-receptor complex with most energetically favourable docking energy was selected for further simulations. For similar starting conformations, the other ligands were aligned with the docked protonated fentanyl using the *RMSD Trajectory Tool* of VMD [21]. The ligand-receptor complexes were placed in 1-palmitoyl-2-oleoyl-sn glycerol-3-phosphatidyl choline (POPC) bilayer models using the CHAMM-GUI *Membrane Builder* [30] (see Fig. 3). MD simulations were performed with GROMACS 2019.5 [1], using the CHARMM36m force-field for the ligands [13], peptides [19] and lipids [23]. The CHARMM TIP3P water model [44] was used as an explicit solvent. Sodium and chloride counterions were added to neutralize the excess charge and attain a salt concentration of 0.15 M. The particle mesh Ewald (PME) method [10] was employed to calculate long-range Coulombic interactions, with a 1.2 nm cut-off for real-space interactions. A force-switch function was implemented for the Lennard-Jones interactions, with a smooth cut-off from 1.0 to 1.2 nm. The temperatures of ligand-receptor complex, membrane lipids, and the water molecules and counterions were coupled separately and maintained at 310 K using the Nosé-Hoover thermostat [18, 38]. System pressure was maintained at 1 bar using the Parrinello-Rahman barostat [39] with a semi-isotropic scheme, where pressure along x-y directions, and the z direction were coupled separately. The coupling constant and compressibility of the barostat were kept at 5 ps and 4.5×10^{-5} bar, respectively. The LINCS algorithm was used to constrain the covalent bonds between hydrogen and other heavy atoms, allowing a simulation time-step of 2 fs [16]. The simulation systems went through successive minimization, equilibration and production runs using the GROMACS scripts generated by the CHARMM-GUI. First, the systems were energy minimized using 1000 steps of steepest descent algorithm, followed by six-step equilibration runs. The first two runs were performed in the NVT (constant particle number, volume, and temperature) ensemble and the remaining runs in the NPT (constant particle number, pressure, and temperature) ensemble. Restraint forces were applied

to the ligand, receptor, lipids, and water molecules, and, z-axis positional restraints were placed on lipid atoms to restrict their motion along the x-y plane. These restraints were gradually reduced during the equilibration process. This procedure leads to different binding modes for the different setups, see Fig. 2. Ultimately, NPT production runs of 1 ns were performed for all systems, with periodic boundary conditions along all three orthonormal directions. Production run trajectories were saved every 10 ps and analysed with GROMACS analysis tools to generate the interatomic distances. VMD software was used for visualization.

2.2 Metadynamics Simulations

A well-tempered metadynamics simulation [2] was performed on a system consisting of a protonated fentanyl ligand and the μ -opioid receptor at pH 7, embedded in a POPC bilayer model. Binding of the ligand at the receptor site was analysed along the funnel pathway [32] of a collective variable (CV) of interest [29]. The z-axis component of the distance between the centre of mass of the terminal carboxylic group carbon atom of ASP147 and the carbon atom between the two nitrogen atoms on the imidazole ring of HIS297, and the nitrogen atom that gets protonated in fentanyl at appropriate pH, was chosen as the CV. A history-dependent biasing potential is applied along the CV for a better sampling of the conformational space, compared to a conventional unbiased MD simulation. Funnel restraint with a radius of 0.9 nm along the xy plane restricts the CV to the region of interest and discourages extensive movement of the ligand in the surrounding ionic aqueous environment. The simulation was performed by GROMACS 2019.5, patched with PLUMED 2.6.0 plugin [5], using a six-step equilibration process as described earlier for the unbiased MD simulations in Sec. 2.1, and with the same force-field and other simulation parameters. Gaussian hills with an initial height of 2 kJ mol⁻¹ were added along the CV and rescaled with a biasing factor of 20 by the metadynamics algorithm. The biasing potential was applied every 1 ps and the Gaussian hill width was kept at 0.1 nm. The binding free energy profiles were generated using the `sum_hills` function of PLUMED and checked for convergence. The production run in a NPT ensemble was allowed to proceed till 100 ns.

2.3 The SQRA Method

We will compute binding rates on the basis of thermodynamics simulations which provide ensemble-based statistical weights for molecular states. The most robust technique known to us and perhaps even the only feasible method to directly relate statistical weights of intermediate steps of a process with transition rates is the square-root approximation approach (SQRA) [15, 31]. In SQRA the system microstates are first clustered by *k*-means. Then, the proportion of microstates belongs to the respective clusters is determined. Transition rates exist only between spatially adjacent clusters. These rates are determined from the square root of the ratio of the occupation numbers of the neighbouring clusters.

The basic idea behind this approach is the following, firstly, it is assumed that after the ligand has reached the location inside the receptor where it “snaps in”, it passes through locally equilibrated states. Regardless of how these ligand states are clustered, the system is locally reversible (based on all state variables). In such an ensemble of molecular system states, the number of ligands leaving a particular cluster at any (instantaneous) time is the same as the number of ligands re-entering the cluster. This behaviour can be imagined as a symmetric matrix. But in which transitions can only occur between clustered system states that are adjacent. Secondly, it is assumed that the rate of transitions between clusters depends only on the equilibrium occupation numbers of the clusters. Then, each entry in this symmetric matrix would be a symmetric function of the cluster occupancy numbers. SQRA assumes that this

function corresponds to the geometric mean of the clusters.

Heida et. al [14] have shown, that this type of discretization of molecular transitions converges to a Fokker-Planck-Equation in the continuous case. Thus, we will compute this SQRA matrix based on the given cluster occupation numbers and treat it as the rate matrix of the molecular process. Then we will apply the PCCA+ method [28] to compute the k_{on} rate of the process based on a Galerkin projection of this matrix.

3 Resulting binding rates

Inflamed tissue is characterised in particular by the fact that the pH value is lower than that of healthy tissue. Hence, the μ -opioid receptors in inflamed tissue (the ones intended to be activated by an opioid) are exposed to an acidic environment, in contrast, the μ -opioid receptors in the brain or gut (the ones not to be activated because of side effects) have a neutral environment.

3.1 Thermodynamic Effects of pH Changes

In general, an acidic pH leads to the protonation of titratable chemical groups that have a pKa value that is above the current pH value. This is not only the case for the opioid (fentanyl or NFEPP) itself, but also for some of the amino acids of the receptor. Especially, histidine with a pKa value of 6.04 is protonated in acidic, inflamed tissue. Fentanyl with a pKa value of 8.4 is protonated in both acid and neutral milieu. NFEPP with a pKa value of 6.82 is only protonated in acidic tissue and is largely deprotonated in neutral milieu. Because of the order of the pKa values, there are three different scenarios for the binding of the opioid to the receptor:

(S1) both the receptor histidines and the opioid molecule are affected by protonation,

(S2) the histidines are deprotonated, but the opioid is still protonated,

(S3) neither the histidines nor the opioid are protonated.

Each of these scenarios occurs with a certain statistical weight w_1, w_2, w_3 as a function of the pH value. Assuming independence between the protonation events, the weights can be calculated from applying the definition of the pKa values:

$$w_1(\text{pH}) := \frac{1}{10^{\text{pH}-6.04} + 1}, \quad (1)$$

$$w_2(\text{pH}) := \frac{1 - w_1}{10^{\text{pH}-pK_{a_{op}}} + 1}, \quad (2)$$

$$w_3(\text{pH}) := 1 - w_1(\text{pH}) - w_2(\text{pH}), \quad (3)$$

where $pK_{a_{op}}$ is the pKa value of the opioid to be analysed. Figures 4 and 5 show the statistical weights of the three scenarios in relation to the pH value for fentanyl and NFEPP.

3.2 Identification of Activation Barriers

We performed MD simulations (see Sec. 2) for the three different scenarios and for both of the opioids. It is known, that the activation of the μ -opioid receptor happens by the opioid docking inside the receptor so that it is positioned between the amino acid histidine (HIS297) and aspartate (ASP147). The receptor is activated by pushing the corresponding helices apart. The opioid binds to ASP147 through electrostatic interaction. Thus, it has to be protonated

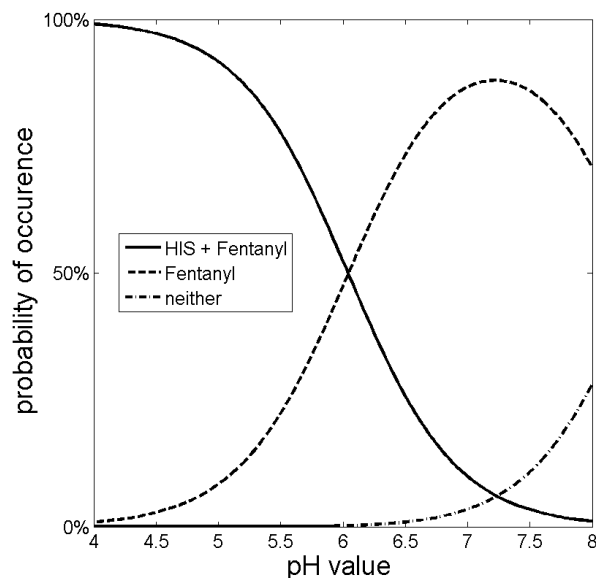


Figure 4: Statistical weights of the three scenarios for fentanyl. Solid line: Histidines and fentanyl are protonated. Dashed line: Only fentanyl is protonated. Dash-dotted line: Neither fentanyl nor histidines are protonated.

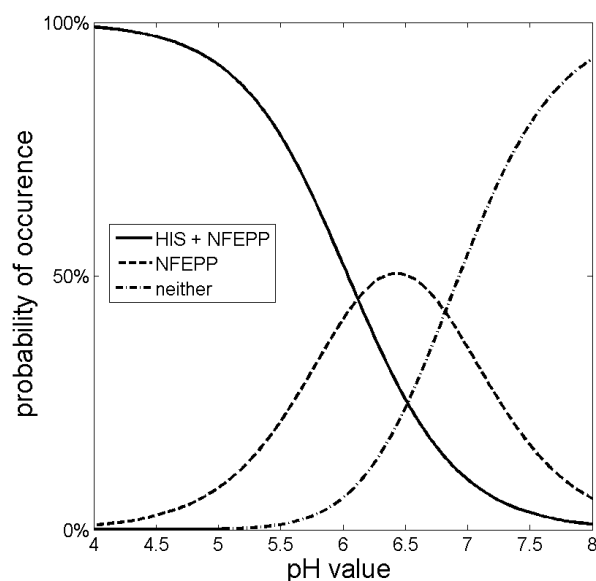


Figure 5: Statistical weights of the three scenarios for NFEPP. Solid line: Histidines and NFEPP are protonated. Dashed line: Only NFEPP is protonated. Dash-dotted line: Neither NFEPP nor histidines are protonated.

to be able to activate the receptor. In our MD simulations, we focused on the interaction behaviour of the two opioids with respect to these two amino acids. Figures 6 and 7 show the statistical distribution of the distances of the opioid to HIS297 and ASP147 during the simulation of the three scenarios described above for fentanyl and NFEPP, respectively.

Comparing the figures, we see that both ligands exhibit a similar qualitative behaviour. In particular, for both ligands, the simulations from *S1* show that the opioid in its binding state comes close to the aspartate but not close to the (equally charged) histidine. When only the opioid is protonated, *S2*, the binding mode is different, and the opioid approaches the histidine

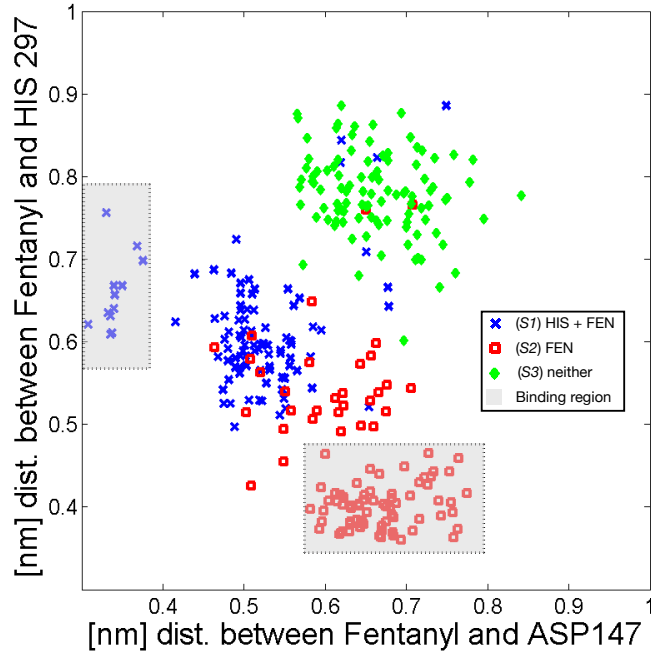


Figure 6: Distance distributions of fentanyl to HIS297 and to ASP147. Crosses: Histidines and fentanyl are protonated. Boxes: Only fentanyl is protonated. Diamonds: Neither fentanyl nor histidines are protonated. Grey rectangular region: binding region.

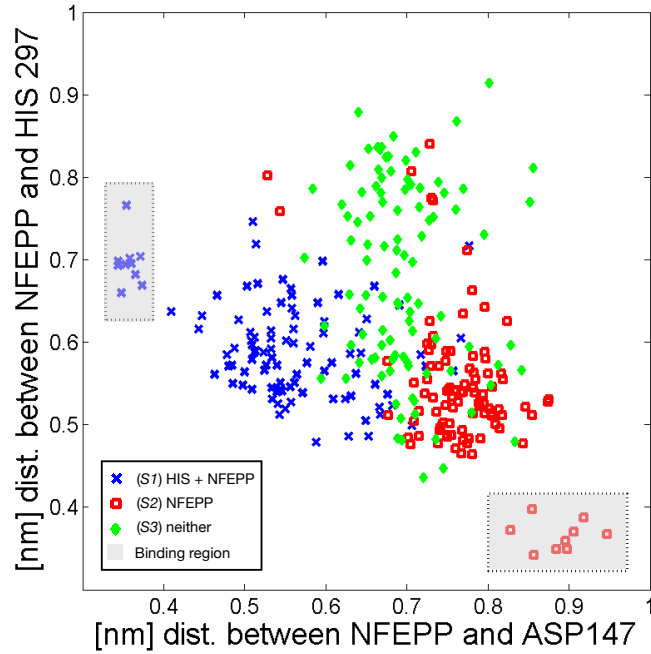


Figure 7: Distance distributions of NFEPP to HIS297 and to ASP147. Crosses: Histidines and NFEPP are protonated. Boxes: Only NFEPP is protonated. Diamonds: Neither NFEPP nor histidines are protonated. Grey rectangular region: binding region.

(in an euclidean sense) more than the aspartate. In *S3*, the opioid does not come close to the aspartate nor to the histidine and, thus, does not activate the receptor.

Besides this qualitative equivalence of the pH-dependant behaviour of fentanyl compared to NFEPP, there are also some differences in the two figures. In *S1*, there is a competition between the positive charge of the HIS297 and the positive charge of the opioid that hinders the opioid from reaching its binding position. There is a clear free energy barrier visible by the

low density of sampling points between the activated state and the “pre”-activated state. It can therefore be assumed, that the binding rate is low (but not zero) in this case. In *S2*, this free energy barrier is also visible for the opioid NFEPP, but not for fentanyl. Thus, we assume, that the binding rate of fentanyl is higher than the binding rate of NFEPP in this case. In *S3*, the binding rate of fentanyl is assumed to be almost zero. The simulation does not show any binding position. Whereas, there might be a very small probability for NFEPP to reach a binding position, because the simulation shows more states which approach the “pre”-activated positions.

3.3 Turning Thermodynamics Into Kinetics

For the computation of the on-rate k_{on} , we first determine a unitless pH-dependent rate κ_{on} . For this we need the cluster occupancy numbers for each scenario separately, i.e., we perform a clustering of the states. These clusters (6 clusters for fentanyl and also for NFEPP) stem from a k -means approach applied to all data points from the three simulations. Six is the smallest number of k -means clusters, where we can distinguish between activated, “pre”-activated and inactive states of the system. In order to compare two different (monovalent) binding modes, we use the mathematical trick from multivalent binding rate estimations [43], where the 2D-coordinates of the data points representing our system microstates are given by, firstly, the minimum of the distance between opioid and HIS297 compared to the distance between opioid and ASP147, and secondly, by the maximum of these two distances. In this way we get a 6-dimensional vector v_1, v_2, v_3 of occupation numbers for each scenario.

In order to now derive a pH-dependent 6×6 -matrix of SQRA-estimated transition rates from our MD simulations, we have to take the weights (Fig. 4 and 5) of the three different scenarios into account. For a given pH value we take the weights w_1, w_2, w_3 and multiply them with the occupation number vectors $v = w_1 v_1 + w_2 v_2 + w_3 v_3$. The resulting vector v defines the entries of the 6×6 -rate matrix by applying SQRA. For estimating the overall transition rate, between *two* macrostates (from inactivated to activated), we compute the Galerkin projection [28] of the SQRA 6×6 -rate matrix to a 2×2 -projection and extract the on-rate from the off-diagonal. The result is shown in Fig. 8. It is called κ_{on} , because there is still one piece of information missing.

The only missing quantity in Fig. 8 is the scaling of the y-axis (i.e., its inverse time unit). This is always the case for SQRA, because it is not possible to derive the time unit from the estimate. However, Fig. 8 reflects exactly our qualitative observations based on the simulation data. It is also in good accordance with experimental findings, that in healthy tissue NFEPP is much less able to activate the μ -opioid receptor than fentanyl and that in inflamed tissue fentanyl and NFEPP have a similar pain relief effect [42]. However, recent MD simulations [24] for the receptor in inflamed tissue, *S1*, imply that self-activation of the μ -opioid receptor may happen more often at low pH. Increased pain suppression may therefore result from self-activation and may not necessarily be due to the opioid binding. Even the off-rates of opioids may be increased at low pH because of (+,+)-Coulomb repulsion effects. Nevertheless, the self-activation effect is independent from the opioid and, thus, still the curves in Fig. 8 imply, that NFEPP and fentanyl should be comparable in receptor activation at low pH due to our simulations. However, this also means that fentanyl should have a stronger overall pain relief effect at low pH than NFEPP, because it activates μ -opioid receptors in the periphery (the inflamed tissue) as well as in the brain, whereas NFEPP only acts at the inflamed periphery. This difference has also been observed experimentally [41]. To now determine the time unit of the y-axis in Fig. 8, we use a result from the literature that says that fentanyl at pH 7.4 has an off-rate of $k_{off} = 5.8 \times 10^{-7} \text{ ms}^{-1}$ [33]. We also know from literature [40], that at pH 7.4 and at a fentanyl concentration of $1.1 \times 10^{-3} \mu\text{M}$ half of the receptors are bound. This means that

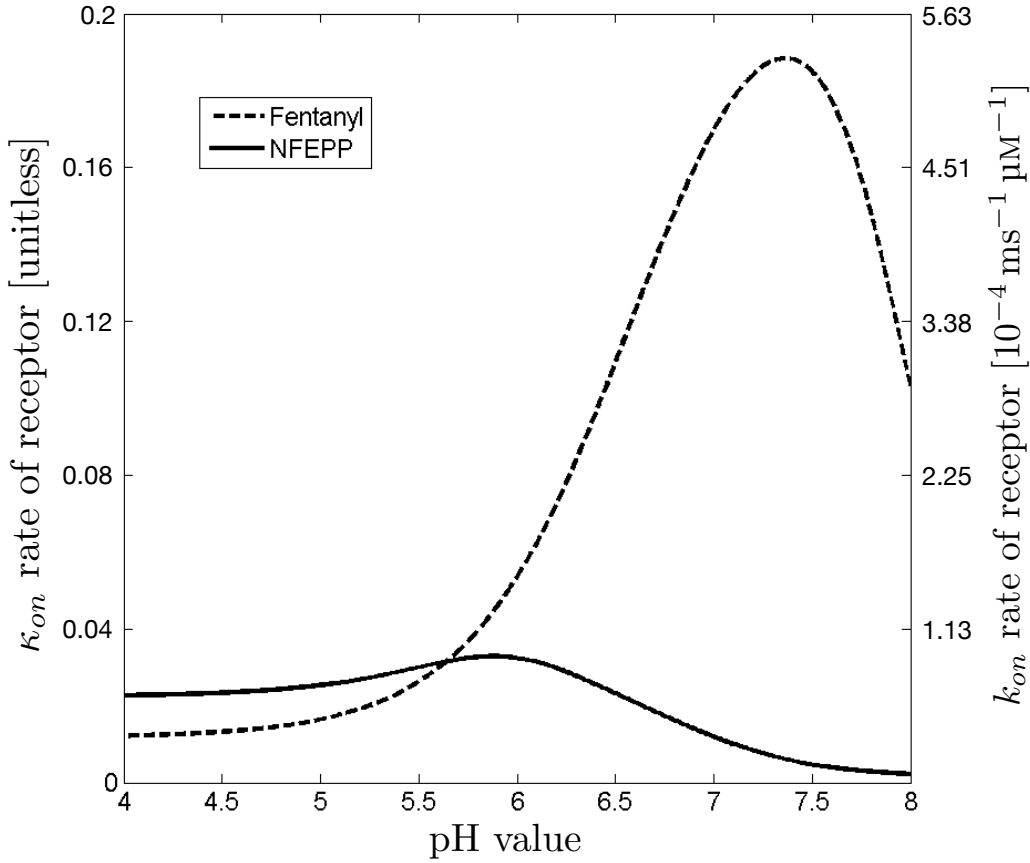


Figure 8: Taking the results from SQRA into account and using the statistical weights of the three scenarios in Fig. 4 and 5 provides a quantitative picture of the changes of binding rates of fentanyl (dashed line) and NFEPP (solid line). Left axis: κ_{on} from SQRA without scaling. Right axis: k_{on} by scaling at pH 7.4.

k_{on} can be calculated for this specific pH via the law of mass action

$$\frac{k_{off}}{k_{on}} = \frac{[R][L]}{[RL]},$$

where $[R]$ is the concentration of unbound receptors, $[RL]$ is the concentration of bound receptors and $[L]$ is the concentration of the ligand (fentanyl). Then, the on-rate for fentanyl at pH 7.4 is given by,

$$k_{on} = \frac{k_{off}}{1.1 \times 10^{-3} \mu\text{M}} = 5.3 \times 10^{-4} \text{ ms}^{-1} \mu\text{M}^{-1}. \quad (4)$$

This defines the scaling of the y-axis, because at pH 7.4 the y-value of the fentanyl curve should be equal to this on-rate. Figure 8 shows that κ_{on} for fentanyl at pH 7.4 was found to be 0.1882 (unitless). Hence, scaling κ_{on} by $c = 2.82 \times 10^{-3} \text{ ms}^{-1} \mu\text{M}^{-1}$ gives us k_{on} in Eq. (4). With the scaling, $k_{on} = c \cdot \kappa_{on}$, we can derive the k_{on} are for the desired pH and opioid from Fig. 8.

4 Application of the MD derived Binding Kinetics

Pharmacodynamic models are mathematical models used to study drug- and disease-dynamics. These mathematical models use the kinetic rates of the drug- target interactions to predict the efficacy of a drug and its putative effects [4, 9, 11, 20, 25]. In practise, these kinetic rates come

from *in vitro* studies which are intricate and highly technical, resulting in only specific conditions being explored. Hence, deriving kinetic rates from MD simulations is a novel alternative, with the potential to explore multiple scenarios and conditions. As a proof-of-concept, we built a pharmacodynamic model [7], using MD derived rates, to reproduce the *in vitro* competitive binding assay performed by Spahn et al. [40], in which they determined the inhibition constants (K_i) of fentanyl and NFEPP for increasing pH levels.

The competitive binding assay in Spahn et al. involved the application of a mixture of a fixed concentration of radioactive DAMGO ligands with variable concentration of competitive ligands to MOR transfected HEK239 cells. After an incubation period, the unbound ligands were washed away. Then the amount of displaced radioactive ligands were calculated by observing the reduction in radioactive decay. The experiment was repeated for different pH regimes, competing ligands (fentanyl and NFEPP), and incubation times. The pharmacodynamic model for this assay is given by the following system of ordinary differential equation (ODEs):

$$\frac{d[R](t)}{dt} = k_{off}^{*,pH} [RL_{\star}](t) + k_{off}^{\bullet,pH} [RL_{\bullet}](t) \quad (5)$$

$$- (k_{on}^{*,pH} [R](t) [L_{\star}](t) + k_{on}^{\bullet,pH} [R](t) [L_{\bullet}](t)) ,$$

$$\frac{d[L_{\star}](t)}{dt} = k_{off}^{*,pH} [RL_{\star}](t) - k_{on}^{*,pH} [R](t) [L_{\star}](t), \quad (6)$$

$$\frac{d[L_{\bullet}](t)}{dt} = k_{off}^{\bullet,pH} [RL_{\bullet}](t) - k_{on}^{\bullet,pH} [R](t) [L_{\bullet}](t), \quad (7)$$

$$\frac{d[RL_{\star}](t)}{dt} = k_{on}^{*,pH} [R](t) [L_{\star}](t) - k_{off}^{*,pH} [RL_{\star}](t), \quad (8)$$

$$\frac{d[RL_{\bullet}](t)}{dt} = k_{on}^{\bullet,pH} [R](t) [L_{\bullet}](t) - k_{off}^{\bullet,pH} [RL_{\bullet}](t), \quad (9)$$

where $[R]$ is the free receptor concentration; $[L_{\star}]$ is the concentration of the radioactive ligand (DAMGO); $[L_{\bullet}]$ is the concentration of the completing ligand of interest (fentanyl or NFEPP); $[RL_{\star}]$ is the concentration of the radioactive ligand bound receptor concentration; and lastly, $[RL_{\bullet}]$ is the concentration of the ligand of interest bound to receptor. The kinetic rates for the ligands at the different pHs are given in Table 1. The superscript of the kinetic rates indicates the ligand and the pH level the rate is associated to. Verbosely, the ligands, $[L_{\star}]$ and $[L_{\bullet}]$, compete for free receptors, $[R]$, to convert them into bound ligand-receptor complexes, $[RL_{\star}]$ and $[RL_{\bullet}]$, at rates $k_{on}^{*,pH}$ and $k_{on}^{\bullet,pH}$, respectively. The bound receptor-ligand complexes, $[RL_{\star}]$ and $[RL_{\bullet}]$, dissociate at rates $k_{off}^{*,pH}$ and $k_{off}^{\bullet,pH}$, respectively.

Before analysing the results of the pharmacodynamic model, we will discuss the kinetic rates which we deduced in Table 1. Firstly, Spahn et al. showed that for NFEPP, the inhibition constant ($K_i = k_{off}/k_{on}$) increases approximately 2.4 fold when the pH is increased from 5.5 to 7.4. However, they could not determine the kinetic rates which induced this fold change. Using the kinetic rates from the MD simulations, we could discern that this increase in the inhibition constant is due to a 5.24 fold decrease in k_{on} and a 2.12 fold increase in k_{off} . Furthermore, Spahn et al. also showed that there were no significant changes in the inhibition constant of fentanyl when pH was increased from 5.5 to 7.4. At first glance, it appears as if pH has no effect on the function of fentanyl. However, when we studied the kinetic rates through the MD simulations, we could see that both the k_{on} and k_{off} rate increase approximately 8 fold as the pH is increased from 5.5 to 7.4. Since both rates change in parallel, we do not see significant changes in the inhibition constants, as inhibition constant in the ratio of the two.

Using the parameters derived in Table 1, we evolved the pharmacodynamic competitive binding model (6–9) inline with the setup by Spahn et al. [40]. Using the EC_{50} of DAMGO given in Spahn et al., we estimated the receptor concentration to be approximately 0.005 nM. The initial DAMGO ligand concentrate was set to 4 nM as performed in Spahn et al. [40]. We

	pH 5.5	pH 6.5	pH 7.4	Units
DAMGO				
k_{on}	$2.04 \times 10^{-4} (*)$	$4.97 \times 10^{-4} (*)$	$4.46 \times 10^{-4} (*)$	$\mu\text{M}^{-1} \text{ms}^{-1}$
k_{off}	(\dagger)	(\dagger)	$5 \times 10^{-7} (\ddagger)$	ms^{-1}
K_d	2.45×10^{-3}	1.01×10^{-3}	1.12×10^{-3}	μM
Fentanyl				
k_{on}	7.4×10^{-5}	3.08×10^{-4}	5.3×10^{-4}	$\mu\text{M}^{-1} \text{ms}^{-1}$
k_{off}	6.79×10^{-7}	4.25×10^{-7}	$5.8 \times 10^{-7} (\ddagger)$	ms^{-1}
K_i	9.18×10^{-4}	1.38×10^{-3}	1.06×10^{-3}	μM
NFEPP				
k_{on}	8.45×10^{-5}	6.5×10^{-5}	1.61×10^{-5}	$\mu\text{M}^{-1} \text{ms}^{-1}$
k_{off}	6.13×10^{-7}	2.4×10^{-7}	2.88×10^{-7}	ms^{-1}
K_i	7.35×10^{-3}	3.67×10^{-3}	1.79×10^{-2}	μM

(\star) The k_{on} rate derived using k_{off}/K_d

(\dagger) The k_{off} rate at pH 7.4 was used

(\ddagger) The k_{off} rates given in Livingston et al. [33]

($_$) K_i , K_d rates given in Spahn et al. [40] for incubation time of 90 min

(k_{on}) rates deduced from Fig. 8

(k_{off}) rates derived using $K_i \times k_{on}$

Table 1: Kinetic Rates deduced from literature and MD simulations

considered eight different initial concentrations of the competing ligand: 5 μM , 1 μM , 0.1 μM , 0.05 μM , 0.01 μM , 0.005 μM , 0.001 μM , 5 $\times 10^{-4}$ μM , and 1 $\times 10^{-8}$ μM . The system was evolved to time $t = 90$ min. This setup was repeated for the competing ligands fentanyl and NFEPP at pH levels of 5.5, 6.5, and 7.4.

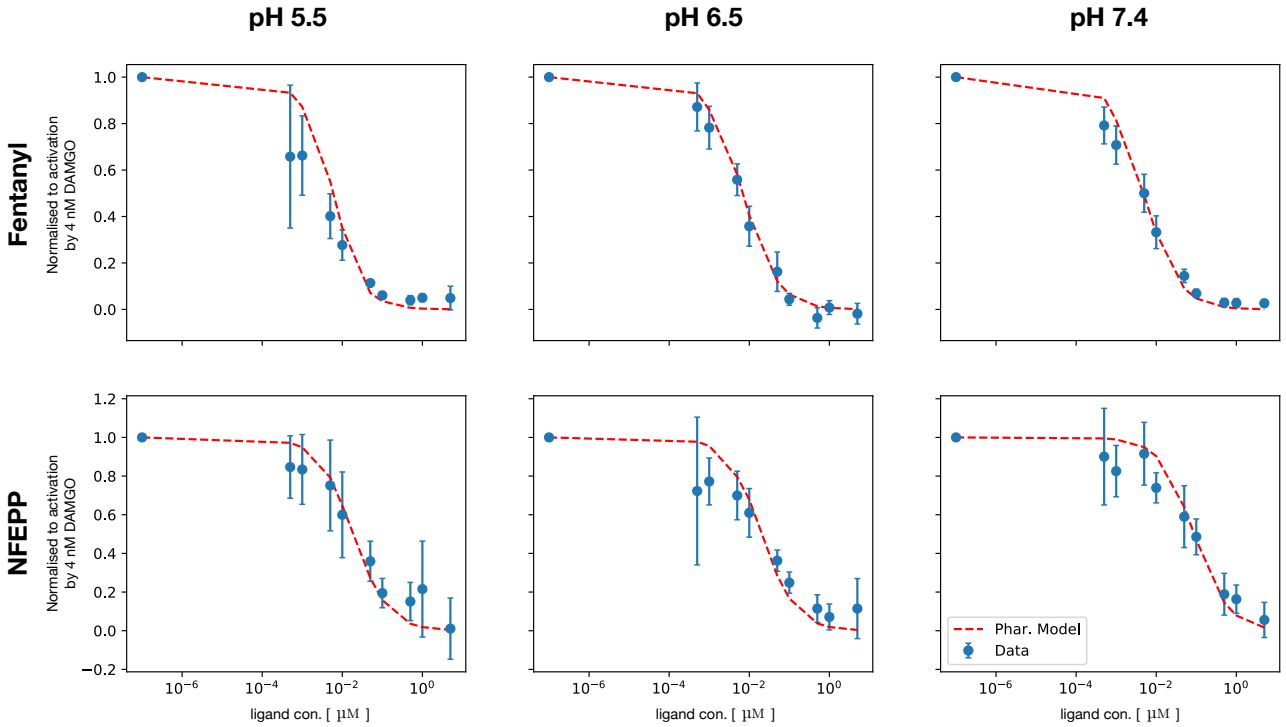


Figure 9: (dashed red line) The pharmacodynamic model of the competitive binding assay using the parameters from Table 1. (blue dot) Data from the *in vitro* competitive binding assay by Spahn et. al. [40], MEAN (\pm STD).

In Figure 9 the solution of the pharmacodynamic competitive binding model is overlaid on the *in vitro* data from Spahn et al. [40]. We see that the pharmacodynamic model captures the ligand competition for concentrations above 0.005 μM . Also the general trend is captured well by the model. However, the model does poorly in capturing the competitive interaction at lower concentrations of the competing ligand. This can be attributed to the approximations which were made to derive the DAMGO kinetics.

In the lower concentrations, DAMGO kinetics are dominant and the dynamics in this concentrations range is sensitive to the accuracy of the kinetic rates. Here we only presented a proof-of-concept to demonstrate the application of the kinetic rates which we derived from MD simulations. In this example, we used the k_{on} rates derived from MD simulations, but the k_{off} rates were deduced from the literature. The natural future research direction would be to formulate a method to estimate the k_{off} rates using the MD simulations. Then, having both k_{on} and k_{off} rates would greatly aid in the study of drug-target interactions and their downstream effects.

5 Discussion/Conclusion

Our novel mathematical approach, which is to combine localised molecular simulations of ligand-receptor interactions in different chemical scenarios with the statistical occurrence of these scenarios, allows an overall view of the pH-dependent kinetics of the system. Even though the effect of pH on these ligands' binding has been investigated *in vitro*, we aimed to give a dynamical interpretation to explain the experimentally observed effects. From our MD simulations, we observed that when the amino acid histidine was protonated (describing a low pH scenario) or fentanyl was deprotonated (describing a high pH scenario), the fentanyl ligand was positioned further away from its normal binding position near HIS297. This could be attributed to repelling or non-attracting Coulomb interactions between the ligand and the amino acid. This could suggest that fentanyl mainly activates central μ -opioid receptors in the brain, when the pain-causing tissue is inflamed and has a low pH value. In contrast to fentanyl, our simulations indicate that NFEPP has a lower preference to bind at pH 7 than at pH 5. This drug molecule was designed for peripheral binding in inflamed tissue (low pH) and avoids receptor activation in the brain (neutral pH). However, from our analysis, we could see that the association rate of NFEPP decays nearly 5-fold when the pH level increases by 2. This suggests that perhaps, as inflamed tissue is rising in its pH level due to healing, an increased concentration of the ligand has to be administered for the same efficacy, indicating to possible mixed opioid treatment strategies [41, 42].

Our novel approach has four key assumptions at its core. Firstly, we extract k_{on} -rates from localised simulations of the system where the ligand is close to its binding position. The assumption is that this last "snap in" step is the rate-determining process for the on-rate. Secondly, we applied the SQRA-method for the rate estimation. This method relies on a clustering of the system states. We assumed that in our clustering, the activation barriers become visible and thus, comparisons between different chemical environments can be done. Thirdly, we assumed that the off-rate of the system is much smaller than the on-rate, which justified its computation on the basis of experimental findings rather than using molecular simulations. Lastly, the pH-dependence of the statistical weights—like in most cases in molecular simulations—is based on mathematical laws which assume well-stirred reaction tubes, which is clearly not the case in human bodies. However, animal testing with fentanyl and its derivatives indicate that the pH-dependence of these drug molecules coincide with their (well-stirred reaction tube) pKa values [42]. Our simulations and pharmacodynamical interpretations may be a good explanation for this observation.

A naturally ensuing future research direction is to start relaxing some the assumptions.

For example, adding in new scenarios such that the k_{off} rate can also be derived by the current pipeline. Furthermore, the conditions that led to the use of the SQRA method can be supplemented by other physical or physico-chemical approaches, so that refined rates can be obtained. Since the SQRA method provides a Markov model, this method can also be combined with other methods that generate Markov models, see e.g. cf. [37], yielding an approach that would allow to abstain from the assumption of the "snap-in step" being rate-limiting. We have demonstrated that mathematically derived rates can be applied to interpret pharmacodynamic measurements. Thus, it is possible to directly correlate pharmacodynamics with the variation of the chemical environment, and consequently, with the variation of binding modes. Further research in this direction will allow for redesigning molecular structures in such a way that the "pharmacodynamical response" to the drug design can be anticipated.

Acknowledgement. This work has partially be funded by the DFG Center of Excellence MATH+, project AA1-1 "The spatio-temporal modelling of mechanisms underlying pain relief via the μ -opioid receptor" and project AA1-6 "Data-driven Modeling from Atoms to Cells", as well as through the grant CRC 1114 (Projects A05 and B05).

References

- [1] M.J. Abraham, T. Murtola, R. Schulz, S. Páll, J.C. Smith, B. Hess, and E. Lindahl. Gromacs: High Performance Molecular Simulations through Multi-Level Parallelism from Laptops to Supercomputers. *SoftwareX*, 1-2:19–25, 2015.
- [2] A. Barducci, G. Bussi, and M. Parrinello. Well-Tempered Metadynamics: A Smoothly Converging and Tunable Free-Energy Method. *Physical Review Letters*, 100:020603, 2008.
- [3] H.-J. Böhm. The Development of a Simple Empirical Scoring Function to Estimate the Binding Constant for a Protein-Ligand Complex of Known Three-Dimensional Structure. *Journal of Computer-Aided Molecular Design*, 8:243–256, 1994.
- [4] Peter L. Bonate. *Pharmacokinetic-Pharmacodynamic Modeling and Simulation*. Springer US, Boston, MA, 2011.
- [5] M. Bonomi, G. Bussi, C. Camilloni, G.A. Tribello, P. Banas, A. Barducci, M. Bernetti, P.G. Bolhuis, S. Bottaro, D. Branduardi, R. Capelli, P. Carloni, M. Ceriotti, A. Cesari, H. Chen, W. Chen, F. Colizzi, S. De, M. De La Pierre, D. Donadio, V. Drobot, B. Ensing, A.L. Ferguson, M. Filizola, J.S. Fraser, H. Fu, P. Gasparotto, F.L. Gervasio, F. Giberti, A. Gil-Ley, T. Giorgino, G.T. Heller, G.M. Hocky, M. Iannuzzi, M. Invernizzi, K.E. Jelfs, A. Jussupow, E. Kirilin, A. Laio, V. Limongelli, K. Lindorff-Larsen, T. Löhner, F. Marinelli, L. Martin-Samos, M. Masetti, R. Meyer, A. Michaelides, C. Molteni, T. Morishita, M. Nava, C. Paissoni, E. Papaleo, M. Parrinello, J. Pfaendtner, P. Piaggi, G. Piccini, A. Pietropaolo, F. Pietrucci, S. Pipolo, D. Provati, D. Quigley, P. Raiteri, S. Raniolo, J. Rydzewski, M. Salvalaglio, G. Sosso, V. Spiwok, J. Sponer, D.W.H. Swenson, P. Tiwary, O. Valsson, M. Vendruscolo, G.A. Voth, and A. White. The, P. c., Promoting Transparency and Reproducibility in Enhanced Molecular Simulations. *Nature Methods*, 16:670–673, 2019.
- [6] G R Bowman, V S Pande, and F Noé, editors. *An Introduction to Markov State Models and Their Application to Long Timescale Molecular Simulation*, volume 797 of *Advances in Experimental Medicine and Biology*. Springer, 2014.

- [7] H Cheng. The influence of cooperativity on the determination of dissociation constants: examination of the Cheng–Prusoff equation, the Scatchard analysis, the Schild analysis and related power equations. *Pharmacological Research*, 50(1):21–40, jul 2004. 397 398 399
- [8] L. Donati, M. Heida, and B.G. Keller and M. Weber. Estimation of the infinitesimal generator by square-root approximation. *J. Phys. Condens. Matter*, 30:425201, 2018. 400 401
- [9] S Duwal, V Sunkara, and M von Kleist. Multiscale Systems-Pharmacology Pipeline to Assess the Prophylactic Efficacy of NRTIs Against HIV-1. *CPT: Pharmacometrics & Systems Pharmacology*, 5(7):377–387, jul 2016. 402 403 404
- [10] U. Essmann, L. Perera, M.L. Berkowitz, T. Darden, H. H. Lee, and L.G. Pedersen. A Smooth Particle Mesh Ewald Method. *J. Chem. Phys.*, 103:8577–8593, 1995. 405 406
- [11] Ene I. Ette and Paul J. Williams, editors. *Pharmacometrics*. John Wiley & Sons, Inc., Hoboken, NJ, USA, mar 2007. 407 408
- [12] J. Gasteiger and M. Marsili. A New Model for Calculating Atomic Charges in Molecules. *Tetrahedron Letters*, 19:3181–3184, 1978. 409 410
- [13] I. Soteras Gutiérrez, F.-J. Lin, K. Vanommeslaeghe, J.A. Lemkul, K.A. Armacost, C.L. Brooks, and A.D. MacKerell. Parametrization of Halogen Bonds in the Charmm General Force Field: Improved Treatment of Ligand–Protein Interactions. *Bioorganic & Medicinal Chemistry*, 24:4812–4825, 2016. 411 412 413 414
- [14] M. Heida, M. Kantner, and A. Stephan. Consistency and convergence for a family of finite volume discretizations of the Fokker–Planck operator. *arXiv*, math.NA 2002.09385, 2020. 415 416
- [15] Martin Heida. Convergences of the squareroot approximation scheme to the Fokker–Planck operator. *Mathematical Models and Methods in Applied Sciences*, 28(13):2599–2635, 2018. 417 418
- [16] B. Hess, H. Bekker, H.J.C. Berendsen, and J.G.E.M. Fraaije. Lincs: A Linear Constraint Solver for Molecular Simulations. *Journal of Computational Chemistry*, 18:1463–1472, 1997. 419 420 421
- [17] T.S. Hofer and S.P. de Visser. *Quantum Mechanical/Molecular Mechanical Approaches for the Investigation of Chemical Systems - Recent Developments and Advanced Applications*. Frontiers Media SA, 2018. 422 423 424
- [18] W. G. Hoover. Canonical Dynamics: Equilibrium Phase-Space Distributions. *Physical Review A*, 31:1695–1697, 1985. 425 426
- [19] J. Huang, S. Rauscher, G. Nawrocki, T. Ran, M. Feig, B.L. de Groot, H. Grubmüller, and A.D. MacKerell Jr. Charmm36m: An Improved Force Field for Folded and Intrinsically Disordered Proteins. *Nature Methods*, 14:71, 2016. 427 428 429
- [20] Edward C. Hulme and Mike A. Trevethick. Ligand binding assays at equilibrium: validation and interpretation. *British Journal of Pharmacology*, 161(6):1219–1237, nov 2010. 430 431
- [21] W. Humphrey, A. Dalke, and K. Schulten. Vmd: Visual Molecular Dynamics. *J. Mol. Graph.*, 14:33–38, 1996. 432 433
- [22] S. Kim, J. Lee, S. Jo, C.L. Brooks Iii, H.S Lee, and W. Im. Charmm-Gui Ligand Reader and Modeler for Charmm Force Field Generation of Small Molecules. *Journal of Computational Chemistry*, 38:1879–1886, 2017. 434 435 436

- [23] J.B. Klauda, R.M. Venable, J. A. J.A. Freites, J.W. O'Connor, D.J. Tobias, C. C. Mondragon-Ramirez, I. Vorobyov, A.D. MacKerell, and R.W. Pastor. Update of the Charmm All-Atom Additive Force Field for Lipids: Validation on Six Lipid Types. *The Journal of Physical Chemistry B*, 114:7830–7843, 2010.
- [24] M. Klimm. *New Strategies in Conformation Dynamics*. Dissertation, FU Berlin/SALSA, 2018.
- [25] W. Klipp, E., Liebermeister and A. Wierling, C., Kowald. *Systems Biology. A Textbook*. Wiley-Blackwell, second edition, 2016.
- [26] S. Klus, F. Nüske, P. Koltai, H. Wu, I. Kevrekidis, C. Schütte, and F. Noé. Data-driven model reduction and transfer operator approximation. *Journal of Nonlinear Science*, 28:985–1010, 2018.
- [27] A. Koehl, H. Hu, S. Maeda, Y. Zhang, Q. Qu, J.M. Paggi, N.R. Latorraca, D. Hilger, R. Dawson, H. Matile, G.F.X. Schertler, S. Granier, W.I. Weis, R.O. Dror, A. Manglik, G. Skiniotis, and B.K. Kobilka. Structure of the μ -Opioid Receptor-Gi Protein Complex. *Nature*, 558:547–552, 2018.
- [28] S. Kube and M. Weber. A Coarse-Graining Method for the Identification of Transition Rates between Molecular Conformations. *J. Chem. Phys.*, 126(2), 2007.
- [29] A. Laio and M. Parrinello. Escaping Free-Energy Minima. *Proc. Natl. Acad. Sci. U.S.A.*, 99:12562–12566, 2002.
- [30] J. Lee, D.S. Patel, J. Stahle, S.-J. Park, N.R. Kern, S. Kim, J. Lee, X. Cheng, M.A. Valvano, O. Holst, Y.A. Knirel, Y. Qi, S. Jo, J.B. Klauda, G. Widmalm, and W. Im. Charmm-Gui Membrane Builder for Complex Biological Membrane Simulations with Glycolipids and Lipoglycans. *Journal of Chemical Theory and Computation*, 15:775–786, 2019.
- [31] H. C. Lie, K. Fackeldey, and M. Weber. A Square Root Approximation of Transition Rates for a Markov State Model. *SIAM. J. Matrix Anal. & Appl.*, 34(2):738–756, 2013.
- [32] V. Limongelli, M. Bonomi, and M. Parrinello. Funnel Metadynamics as Accurate Binding Free-Energy Method. *Proceedings of the National Academy of Sciences*, 110:6358, 2013.
- [33] Kathryn E Livingston, Jacob P Mahoney, Aashish Manglik, Roger K Sunahara, and John R Traynor. Measuring ligand efficacy at the mu-opioid receptor using a conformational biosensor. *eLife*, 7, jun 2018.
- [34] D.T. Manallack, R.J. Prankerd, E. Yuriev, T.I. Oprea, and D.K. Chalmers. The significance of acid/base properties in drug discovery. *Chem Soc Rev.*, 42(2):485-496, 2013.
- [35] G. M. Morris, R. Huey, W. Lindstrom, M.F. Sanner, R.K. Belew, D.S. Goodsell, and A.J. Olson. Autodock4 and Autodocktools4: Automated Docking with Selective Receptor Flexibility. *Journal of Computational Chemistry*, 30:2785–2791, 2009.
- [36] G.M. Morris, D.S. Goodsell, R.S. Halliday, R. Huey, W.E. Hart, R.K. Belew, and A.j. Olson. Automated Docking Using a Lamarckian Genetic Algorithm and an Empirical Binding Free Energy Function. *Journal of Computational Chemistry*, 19:1639–1662, 1998.
- [37] Plattner N, Doerr S, De Fabritiis G, and Noe F. Complete protein-protein association kinetics in atomic detail revealed by molecular dynamics simulations and Markov modelling. *Nat Chem.*, 9(10):1005-1011, 2017.

- [38] S. Nosé. A Molecular Dynamics Method for Simulations in the Canonical Ensemble. *Molecular Physics*, 52:255–268, 1984. 478 479
- [39] M. Parrinello and A. Rahman. Polymorphic Transitions in Single Crystals: A New Molecular Dynamics Method. *Journal of Applied Physics*, 52:7182–7190, 1981. 480 481
- [40] V. Spahn, G. Del Vecchio, D. Labuz, A. Rodriguez-Gaztelumendi, N. Massaly, J. Temp, V. Durmaz, P. Sabri, M. Reidelbach, H. Machelska, M. Weber, and C. Stein. A non-toxic pain killer designed by modeling of pathological receptor conformations. *Science*, 355(6328):966–969, 2017. 482 483 484 485
- [41] V. Spahn, G. Del Vecchio, A. Rodriguez-Gaztelumendi, J. Temp, D. Labuz, M. Kloner, M. Reidelbach, H. Machelska, M. Weber, and C. Stein. Opioid receptor signaling, analgesic and side effects induced by a computationally designed pH-dependent agonist. *Scientific Reports*, 8(8965), 2018. 486 487 488 489
- [42] G. Del Vecchio, D. Labuz, J. Temp, V. Seitz, M. Kloner, R. Negrete, A. Rodriguez-Gaztelumendi, M. Weber, H. Machelska, and C. Stein. pKa of opioid ligands as a discriminating factor for side effects. *Scientific Reports*, 9:19344, 2019. 490 491 492
- [43] M. Weber, A. Bujotzek, and R. Haag. Quantifying the rebinding effect in multivalent chemical ligand-receptor systems. *Journal of Chemical Physics*, 137(5):054111, 2012. 493 494
- [44] W. L. W.L. Jorgensen, J. Chandrasekhar, J.D. Madura, R.W. Impey, and M.L. Klein. Comparison of Simple Potential Functions for Simulating Liquid Water. *J. Chem. Phys.*, 79:926–935, 1983. 495 496 497
- [45] H. Wu and F. Noe. Variational approach for learning Markov processes from time series data. *Journal of Nonlinear Science*, 30(1):23–66, 2020. 498 499